Upstream and downstream influence on the unsteadiness of STBLI using DNS data in two configurations

M. Pino Martin,* S. Priebe,† and M. Wu‡

Department of Mechanical and Aerospace Engineering

Princeton University, Princeton, NJ 08544

Statistical analysis of the upstream and downstream flow influence on shock unsteadiness in shock and turbulent boundary layer interactions are performed using DNS data of a compression corner Wu & Martin[1] and a reflected shock case interaction. For both cases, the scaling proposed by Dussauge et al.[2] for the characteristic low frequency applies. The statistical analysis for the compression corner shows that the unsteadiness of the shock is dominated by the downstream flow. The same analysis applied to the reflected shock case also indicates downstream influence. Additional studies are required to fully characterize the reflected shock case DNS data.

I. Introduction

One of the key features of shock wave and turbulent boundary layer interaction (STBLI) is the unsteady motion of the shock. For two dimensional interactions, such as those considered here, the shock translates in the streamwise direction with translation magnitude of O(δ) and with a smaller wrinkling motion superimposed.[3,1,4] Our DNS data of in a compression corner configuration[1] is consistent with these experimental observations.[5] The spanwise wrinkling is caused by the upstream boundary layer structures convecting throught the shock.[6] Presently, there are two schools of thought that try to explain the cause for the translation motion, namely being given by: (a) the upstream boundary layer, more recently 'superstructures'[7,6,8,3] and (b) the downstream separated flow.[9]

Recent analyses using the DNS data of Wu & Martin[1] for a compression corner configuration with incoming boundary layer at Mach 3 and Retheta 2300 show that the shock unsteadiness is driven by the downstream flow.[5] Dussauge, Dupont & Debiéve[2] define a Strouhal number based on the separation length and free stream velocity. They find that experimental data covering a range of Mach number, Reynolds numbers and various configurations can be grouped in St_L=0.02 and 0.05. Wu & Martin[5] find St_L= 0.03-0.042. Wu & Martin[5] also find that redefining the Strouhal number using a characteristic velocity for the separated flow (average maximum reversed flow velocity), the Strouhal number is close to unity, St_{Ur}=0.8.

In this paper, we present new analyses to further study the upstream and downstream flow influence on shock unsteadiness using direct numerical simulation (DNS) data in two configurations. In what follows, we present the flow configurations and flow conditions, the wall-pressure data and the data analyses.

II. Numerical simulations

The conservation equations for mass, momentum and energy are solved in generalized curvilinear coordinates. The numerical method consists of a 4th order accurate linear and non-linear optimized WENO scheme for the convective fluxes,[10] 4th order accurate central finite difference scheme for the viscous fluxes and a

---

*Assistant Professor, Senior Member `pmartin@princeton.edu`

†Ph.D., Student Member AIAA.

‡Ph.D., Student Member AIAA.

3rd order accurate Runge-Kutta method for the time integration. The initial conditions are implemented as in Martin[11] and a recycling boundary condition is implemented at the inflow.[12]

Figure 1 shows inviscid flow schematics for the configurations considered, namely a compression corner interaction with compression angle of 24° (fig. 1a) using the existing DNS data of Wu & Martin[1] and a reflected shock interaction using a free stream flow deflection of 12°, for which we introduce new DNS data. Analytical transformations are used to generate the grids. Sample grids are shown in figure 2 for both configurations. The grids are clustered near the corner or impingement region and in the wall-normal direction. The size of the computational domains is shown in fig. 3, with 1024x160x128 and 1100x160x132 grid point in the streamwise, spanwise and wall-normal directions for figures 3a and b, respectively.

The incoming boundary layer is the same for both calculations at Mach 3 and Retheta 2400.

III. Wall-pressure signals

A. Compression corner case

The mean wall-pressure distribution for the DNS and experimental data[13] for the same configuration and flow conditions is given in fig. 4a, showing good agreement. The error bars show an estimated experimental error of 5%. The corner is located at x=0. Figure 4b plots the magnitude of wall-pressure fluctuations from the DNS data and experiments.[14] There is good agreement between the DNS and experimental data, except that the DNS gives slightly higher magnitude. This is because the synthetically generated turbulence structures in the initial DNS condition produce slightly higher levels of uncorrelated pressure fluctuations, or noise, in the incoming boundary layer. Thus, the fluctuating wall pressure in the DNS is the sum of the actual value, p'_w, and that due to uncorrelated noise, p'_n, and $\overline{(p'_w + p'_n)^2} \approx \overline{p'^2_w} + \overline{p'^2_n}$, since $2\overline{p'_w p'_n}$ can be neglected. An estimate of the noise level can be obtained using the free stream value, p'_∞, upstream and downstream of the shock interaction region. The mean squared of the pressure fluctuations is about 0.04% and 0.16% upstream and downstream of the shock, respectively. Taking the square root of these values gives an amplification factor 2, and an rms noise value of 2% and 4% upstream and downstream of the interaction, respectively. These estimates give good approximations of the differences between the DNS and experimental data shown in fig. 4b. The histograms of the wall-pressure signals for the DNS and experimental data at matching conditions are shown in fig. 5. The DNS data is low-pass filtered at 50 kHz to match the resolution of the experiment for comparison. Figure 6 plots the pre-multiplied energy spectral density for the wall pressure given by the same DNS and experiments in three streamwise locations: in the undisturbed boundary layer, at the mean separation and at the first peak in the magnitude of wall-pressure fluctuation. U_∞/δ is 95 kHz for the DNS and 95 kHz for the experiments. The agreement among the simulation and experimental data is good, with the magnitudes in the DNS data being slightly higher. For streamwise locations within the separation region the data of both studies show low-frequency peaks at similar locations 0.6-1.2 kHz for DNS and 0.6-0.8 kHz for the experiment. These low peaks correspond to the characteristic low frequency of the shock motion. Both numerical and experimental spectra exhibit peaks at high frequencies (of order 105 kHz), with disagreement between the peak locations of the DNS and the experiments. This is due to a combination of effects, namely the low-pass filtering of the experimental signal, which determines the maximum frequency resolution at about 17 kHz,[14] and the effect of the characteristic forcing frequency imposed by the rescaling method at about 21 kHz.[15]

B. Reflected shock case

Bookey et al.[13] gathered experimental data for the reflected shock case for the same incoming boundary layer flow conditions and free stream deflection angle as those used in the DNS. They found significant three-dimensional effects imposed by the side walls in the experiment. Figure 7 shows surface oil visualizations from the experiment and a schematic drawing of the near-wall flow pattern. The three-dimensionality imposed by the experimental side walls affects the flow downstream of the separation point and the wall-pressure. The computer power required to simulating the entire experimental span and the side walls renders such calculations impossible today. Thus, comparing the DNS and experiment data is not sensible since the configurations are different. The numerical method is general and robust and has been applied to a variety of shock interaction problems over a range of conditions without modification,[1,10,16] allowing us to proceed with confidence in the calculation of the reflected shock interaction. Figure 8a plots the wall-pressure signals for the DNS data at different streamwise locations, incoming boundary layer, mean separation point and

American Institute of Aeronautics and Astronautics Paper 2008-0719

inside the separated region. The signals resemble those for the compression corner case. Figure 8b plots the pre-multiplied energy spectral density for the wall pressure signals. The peaks associated with the characteristic low and high frequencies are about 0.15-0.5 kHz and 17-40 kHz, respectively. The scaling proposed by Dussauge et al, $St_l = fL_\text{sep}/U_\infty$, together with the DNS data for the compression corner can be used to obtain a theoretical estimate for the characteristic low-frequency of shock motion in the reflected shock case. Figure 9 plots the skin friction coefficient for the compression corner and reflected shock case DNS data, with x=0 at the separation point. The size of the separation region for the reflected shock case is about 1.82 times that of the compression corner case. Using the scaling, the low frequency for the reflected shock case is 1/1.82 that for the compression corner, or about 0.3-0.7 kHz, which is close to the values given by the DNS.

IV.   Upstream and downstream influence

To study the effect of the upstream and downstream influence on the shock unsteadiness, we consider the co-spectrum of the mass-flux signal in the boundary layer and the pressure signal at the mean shock location. In high Reynolds number flows, the shock location is inferred from wall-pressure measurements. In contrasts at low Reynolds number, such as that considered here, the shock does not penetrate as deeply in to the boundary layer as for high Reynolds number flow, and the shock location is not well defined in the lower half of the boundary layer.[1] For this reason, we perform the co-spectrum analysis for the signals measured at $z_n = 0.7\delta$.

A.   Compression shock case

Figure 10a shows the location were the signals have been measured. Figure 10b plots the corresponding co-spectrum showing that the upstream flow and the shock motion are most correlated at a high frequency. Figure 11 shows the data for the co-spectrum between the shock motion and the downstream flow at the reattachment point and two locations downstream of it. For the signals, characteristic flow frequencies of about 0.65-1.2 kHz. For the signals downstream of the reattachment, characteristic high frequencies of about 21 kHz are also apparent, but not for the reattachment point. The high-frequency corresponds to that of the recycled structures. Figure 12 plots the coherency functions for the shock location with the separation and reattachment points, showing perfect correlation at the low frequencies.

B.   Reflected shock case

Similarly for the compression corner, fig. 13 plots the coherency function for the correlation coefficient between the momentum signals upstream and downstream of the interaction and the pressure signal at the shock location. For the upstream data, no particular characteristic low frequency is observed. For the downstream data, a clear peak is observed at 0.5 kHz, which corresponds with the low frequency shock motion.

V.   Conclusion

The upstream and downstream flow influence on shock unsteadiness has been investigated using the DNS data of Wu & Martin[1] for a compression corner and new DNS data for a reflected shock configuration. Experimental data is used to validate the DNS for the compression corner. The wall-pressure signals are used to infer the characteristic low and high frequencies of shock motion. The low-frequencies are consistent with the predictions given by the Dussauge et al.[2] scaling. Studying the correlation between the momentum in the upstream and downstream boundary layer and the pressure signal at the shock location in frequency space for the compression corner indicates that the low-frequency shock motion is dominated by the downstream flow. The same conclusion is found when the analysis is applied to the reflected shock case. Further analyses are required to fully characterize the data for the reflected shock case.

VI.   Acknowledgments

References

[1]Wu, M. and Martin, M. P., "Direct numerical simulation of shockwave and turbulent boundary layer interaction induced by a compression ramp," *AIAA Journal*, Vol. 45, No. 4, 2007.

[2]Dussauge, J., Dupont, P., and Debieve, J., "Unteadiness of shock wave boundary layer interaction with separation," *Aerospace Science and Technology*, Vol. 10, 2006.

[3]Ganapathisubramani, B., Clemens, N., and Dolling, D., "Effects of upstream boundary layer on the unsteadiness of shock induced separation," *Journal of Fluid Mechanics*, Vol. 585, 2007, pp. 369–394.

[4]Wu, P., Lempert, W., and Miles, R., "Megahertz pulse-burst laser and visualization of shock-wave/boundary layer interaction," *AIAA Journal*, Vol. 38, 2000, pp. 672–679.

[5]Wu, M. and Martin, M. P., "Analysis of shock motion in shockwave and turbulent boundary layer interaction using direct numerical simulation data," *Journal of Fluid Mechanics*, Vol. 594, 2008, pp. 71–83.

[6]Erengil, M. and Dolling, D., "Correlation of separation shock motion with pressure fluctuations in the incoming boundary layer," *AIAA Journal*, Vol. 29, 1991, pp. 1868–1877.

[7]Andreopoulos, J. and Muck, K., "Some new aspects of the shock-wave/boundary layer interaction in compression-ramp flows," *Journal of Fluid Mechanics*, Vol. 180, 1987, pp. 405–428.

[8]Beresh, S., Clemens, N., and Dolling, D., "Relationship between upstream turbulent boundary layer velocity fluctuations and separation shock unsteadiness," *AIAA Journal*, Vol. 40, 2002, pp. 2412–2423.

[9]Thomas, F., Putnam, C., and Chu, H., "Turbulent boundary layer separation," *Experiments in Fluids*, Vol. 18, 1994, pp. 69–81.

[10]Taylor, E., Wu, M., and Martin, M., "Optimization of Nonlinear Error Sources for Weighted Non-Oscillatory Methods in Direct Numerical Simulations of Compressible Turbulence," *Journal of Computational Physics*, Vol. 223, 2007, pp. 384–397.

[11]Martin, M., "DNS of Hypersonic Turbulent Boundary Layers. Part I: Initialization and Comparison with Experiments," *Journal of Fluid Mechanics*, Vol. 570, 2007, pp. 347–364.

[12]Xu, S. and Martin, M., "Assessment of inflow Boundary Conditions for Compressible Turbulent Boundary Layers," *Physics of Fluids*, Vol. 16, 2004, pp. 2623–2639.

[13]Bookey, P., Smits, A., and Martin, M., "New Experimental Data of STBLI at DNS/LES Accessible Reynolds Numbers," *AIAA Paper No. 2005-0309, 43rd AIAA Aerospace Science Meeting and Exhibit, Reno, NV*, January 2005.

[14]Ringuette, M. and Smits, A., "Wall-Pressure Measurements in a Mach 3 Shock-Wave Turbulent Boundary Layer Interaction at a DNS-Accessible Reynolds Number," *AIAA Paper No. 2007-4113*, June 2007.

[15]Martin, M. and Wu, M., "Upstream and Downstream influence on the unsteadiness of STBLI using DNS Data," *Proceedings of the IUTAM Symposium on Unsteady Separated Flows and their Control, Corfu, Greece, June*, 2007.

[16]Taylor, E., Grube, N., and Martin, M., "Evaluation of traditional and shock-confining LES filters using data of compressible turbulence," *AIAA Paper 2007-4197, 37th AIAA Fluid Dynamics Conference and Exhibit, Miami, FL*, June 2007.

[17]Bookey, P., *An Experimental Study of Shock/Turbulent Boundary Layer Interactions at DNS Accessible Reynolds Numbers*, Master's thesis, Princeton University, 2005.
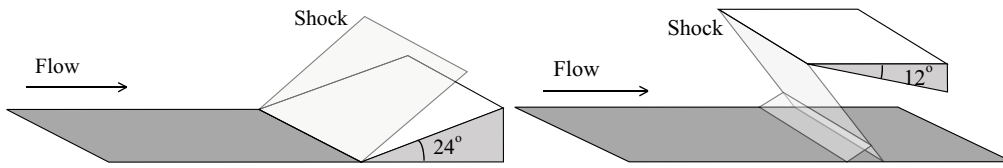
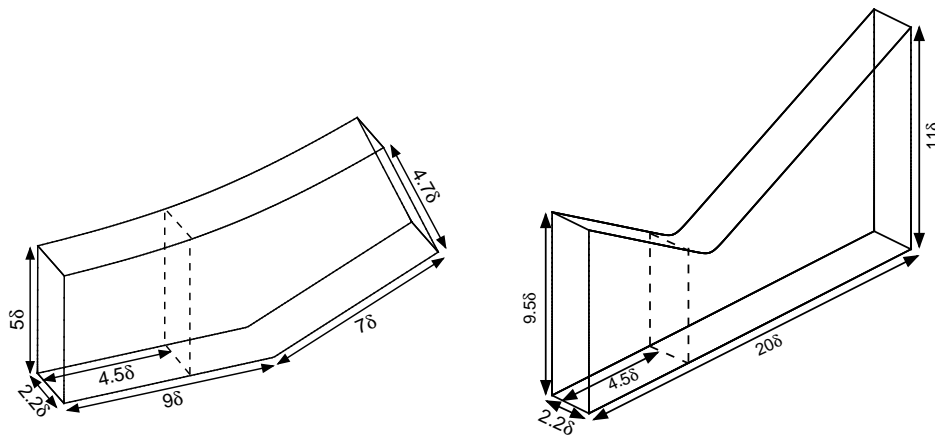Figure 1. Flow configurations for the DNS.
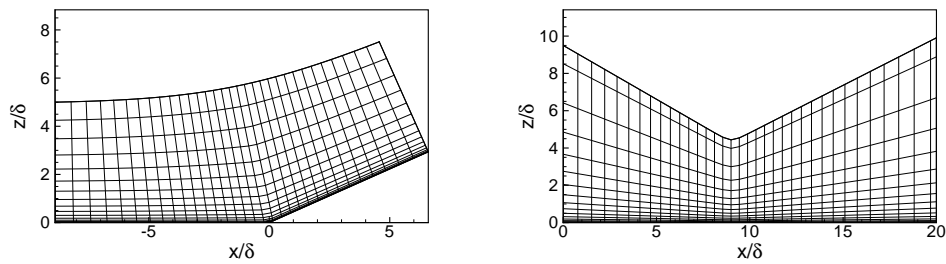

Figure 2. Computational domains for the DNS.

Figure 3. Sample grids for the DNS.

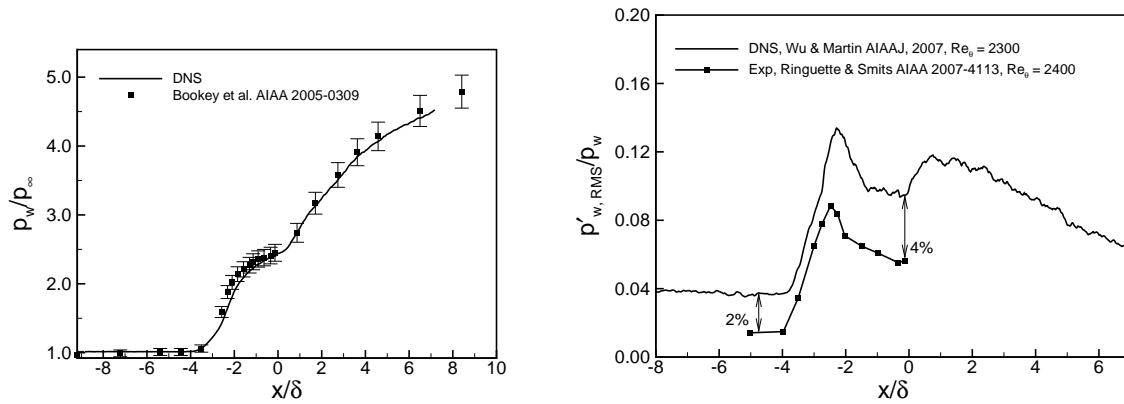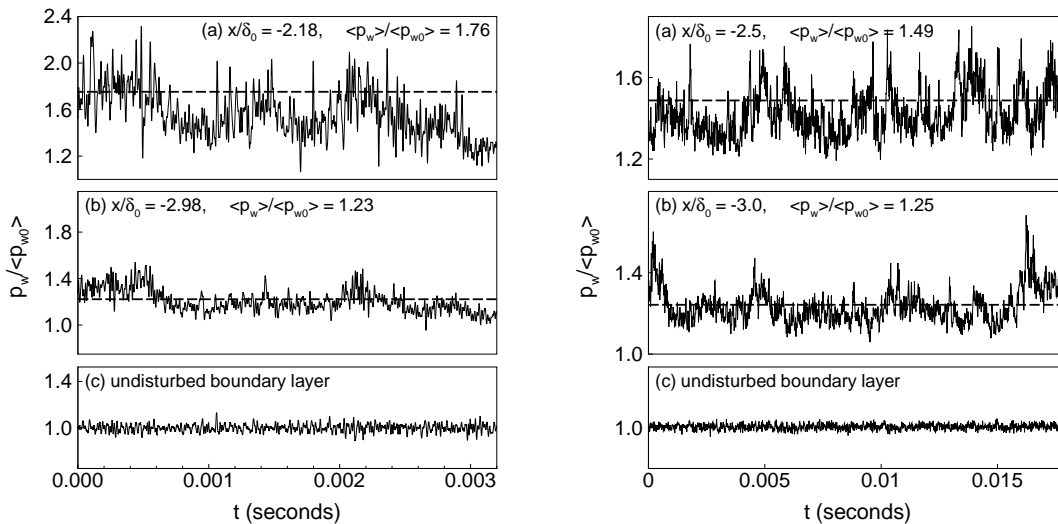American Institute of Aeronautics and Astronautics Paper 2008-0719

Figure 4. Wall-pressure distributions for the compression corner case. (a) Mean from DNS and experiment[13] (adapted from Wu & Martín[1]) and (b) rms from DNS[1] and experiments. Experiments match the flow configurations and conditions of the DNS

.

(a) Adapted from Wu & Martín.[1]

(b) Adapted from Ringuette & Smits.[14]

Figure 5. Comparison of wall-pressure signals. Plot ordinates have been scaled so that signal strengths are comparable. (a) DNS data from Wu and Martín;[1] (b) Experimental data from Ringuette & Smits.[14] DNS data have been low-pass filtered at a cutoff frequency of $f\delta_0/U_\infty = 0.55$, to match the resolution of the experiment. The time axis of the DNS plot has been stretched due to the smaller number of available samples. Dashed lines indicate mean values.
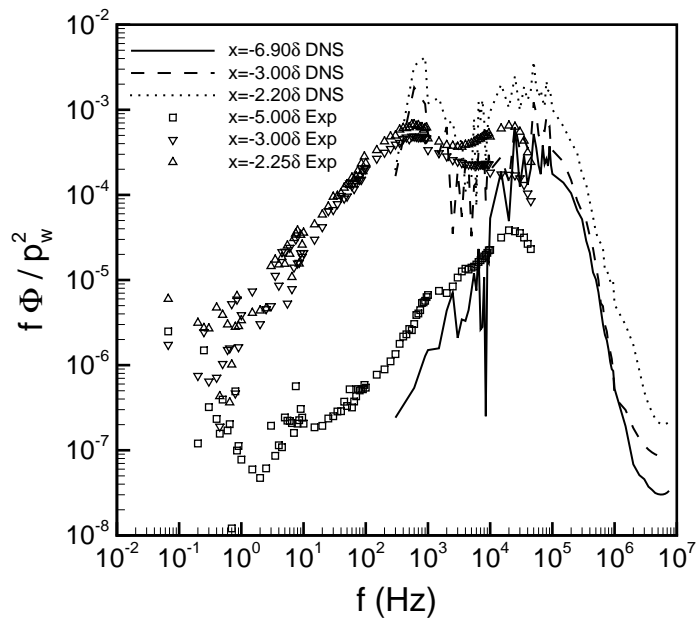
Figure 6. Pre-multipled energy spectral density for the wall-pressure signal at different streamwise locations. Lines for the DNS[1] and symbols for the experiments[14] at matching conditions. The streamwise locations correspond to the incoming boundary later, mean separation point, and the peak in the wall p'_{RMS} curve, respectively.
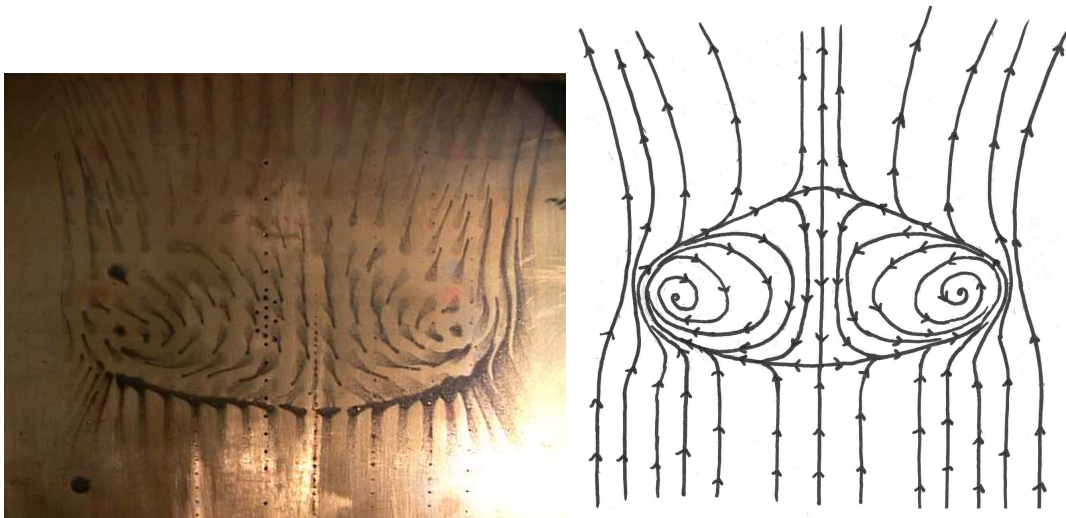

Figure 7. Surface (a) flow pattern from experiment and (b) schematic for the 12° reflected shock interaction at Mach 2.9 and $Re_\theta = 2300$. Adapted from Bookey[17]
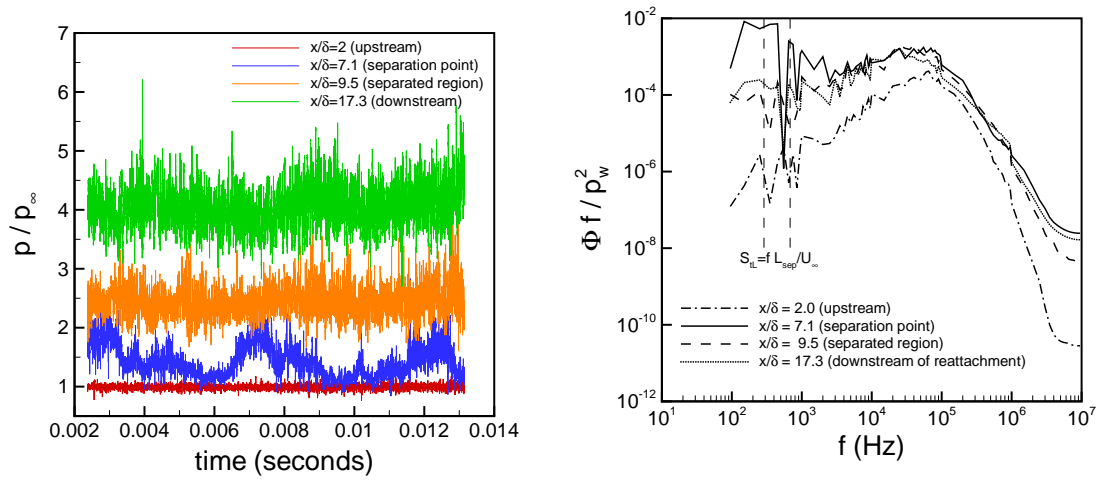
Figure 8. (a) Wall-pressure signal and (b) pre-multipled energy spectral density for the wall-pressure signal for the reflected shock case at different streamwise locations from DNS.
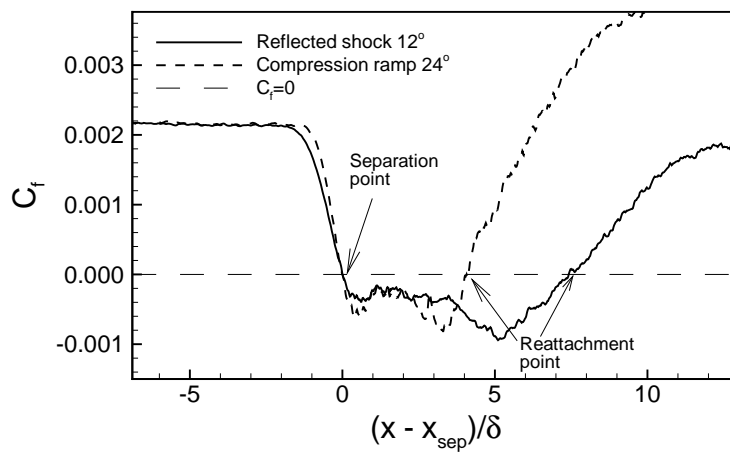

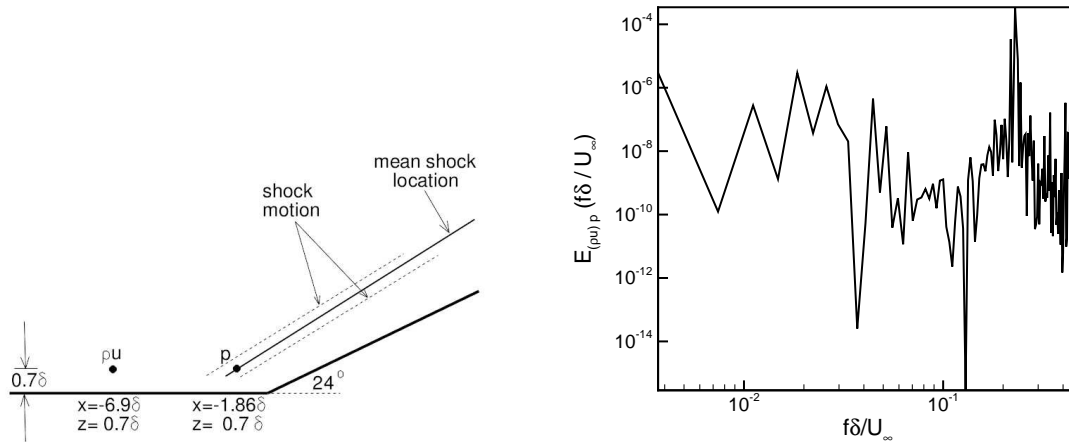**Figure 9.** Skin friction coefficient from DNS.

Figure 10. Spanwise averaged, pre-multiplied co-spectrum between the mass-flux in the incoming boundary layer at $(x = -6\delta, y, z_n = 0.7\delta)$ and the pressure at the mean shock location $(x_{\text{shock}}, y, z_n = 0.7\delta)$. (a)Sketch showing the locations for measurement and (b) data. From Martin & Wu[15]
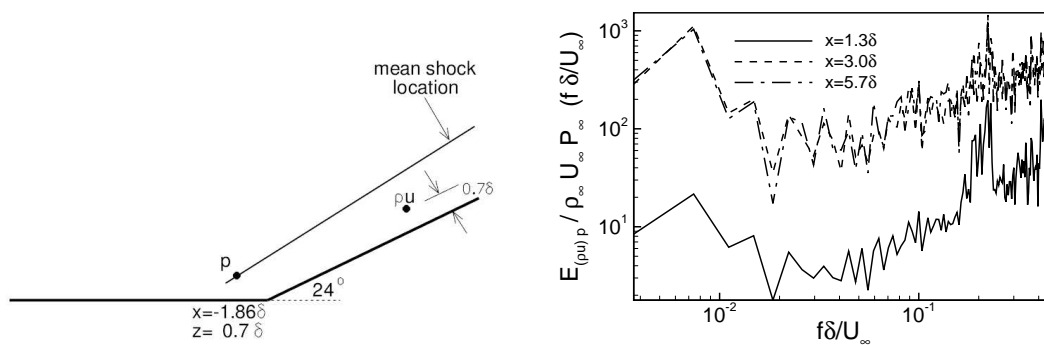

Figure 11. Spanwise averaged, pre-multiplied co-spectrum between the mass-flux in the boundary layer downstream of the interaction and reattachment $(x = 1.3\delta)$ and two other locations downstream of the reattachment point with $(z_n = 0.7\delta)$ and the pressure at the mean shock location $(x_{\text{shock}}, y, z_n = 0.7\delta)$ for the compression corner from DNS. (a) Sketch showing the locations of measurement and data. From Martin & Wu[15]
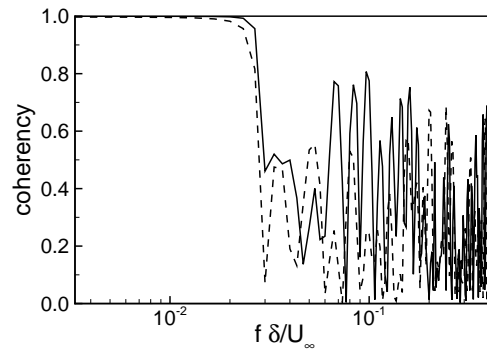

Figure 12. Coherency function between the spanwise-mean shock location at $z_n = 2\delta$ and (solid line) spanwise-mean separation point and (dashed line) spanwise-mean reattachment point. From Martin & Wu[15]
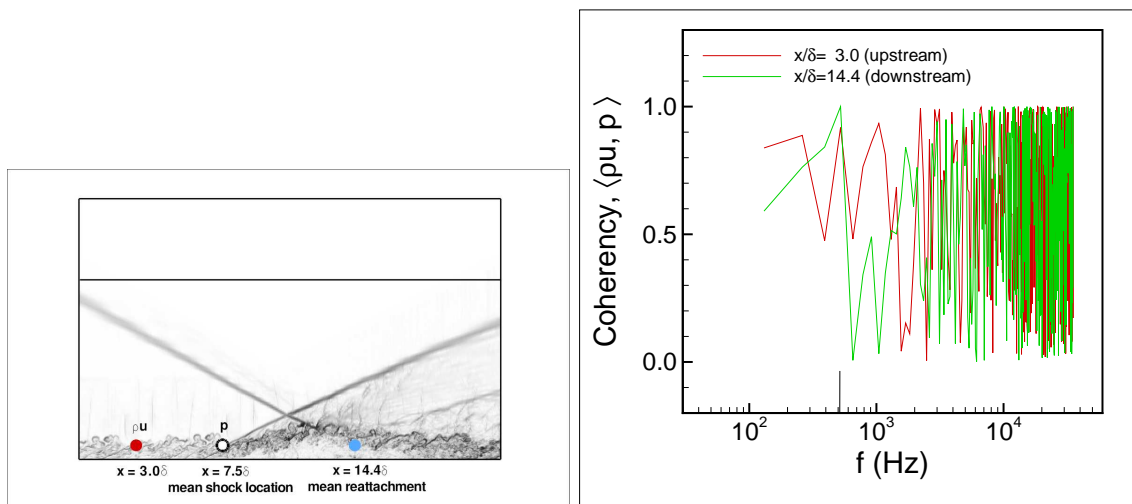
Figure 13. Spanwise averaged, pre-multiplied co-spectrum between the mass-flux in the incoming boundary layer at $(x = 3\delta, y, z_n = 0.7\delta)$ **and the pressure at the mean shock location** $(x_{\text{shock}}, y, z_n = 0.7\delta)$ **for the reflected shock case from DNS. (a)Sketch showing the locations for measurement and (b) data.**